

High T_c superconductivity in $\text{CaKFe}_4\text{As}_4$ in absence of nematic fluctuations

W.-L. Zhang,^{1,*} W. R. Meier,^{2,3} T. Kong,^{2,3} P. C. Canfield,^{2,3} and G. Blumberg^{1,4,†}

¹*Department of Physics & Astronomy, Rutgers University, Piscataway, New Jersey 08854, USA*

²*Department of Physics and Astronomy, Iowa State University, Ames, Iowa 50011, USA*

³*Division of Materials Science and Engineering, Ames Laboratory, Ames, Iowa 50011, USA*

⁴*National Institute of Chemical Physics and Biophysics, Akadeemia tee 23, 12618 Tallinn, Estonia*

(Dated: April 20, 2018)

We employ polarization-resolved Raman spectroscopy to study multi-band stoichiometric superconductor $\text{CaKFe}_4\text{As}_4$. The B_{2g} symmetry Raman response shows no signatures of Pomeranchuk-like electronic nematic fluctuations which is observed for many other Fe-based superconductors. In the superconducting state, we identify three pair-breaking peaks at 13.8, 16.9 and 21 meV and full spectral weight suppression at low energies. The pair-breaking peak energies in Raman response are about 20% lower than twice the gap energies as measured by single-particle spectroscopy, implying a sub-dominant d -wave symmetry interaction. We analyze the superconductivity induced phonon self-energy effects and give an estimation of weak electron-phonon coupling constant $\lambda^\Gamma=0.0015$.

Introduction – Understanding the pairing mechanism in the Fe-based superconductors (FeSC) remains focused topic of research not only due to a high superconducting transition temperature T_c , but also because of the unusual properties and interplay with other electronic degrees of freedom, such as nematicity and magnetism [1–6]. For FeSCs, superconductivity usually appears in close proximity to nematic and/or magnetic ground states [4, 7].

FeSCs are believed to be unconventional superconductors because the pairing mechanism is due to electronic rather than phononic interactions. It has been proposed that spin-fluctuation can lead to s_\pm symmetry pairing with sign reversal gap function between Fermi surface (FS) pockets around Γ and M point [8, 9]. In addition, strong electronic nematic fluctuations have been observed for the materials with highest T_c [10–12] and, hence, a mechanism for T_c enhancement by nematic fluctuations has been proposed [13]. As the alternatives, orbital-fluctuation in the presents of strong electron-phonon interaction were considered to be another possible pairing glue which could lead to nodeless s_{++} symmetry pairing [14–16]. Raman scattering has been used to study the spectroscopy of superconducting (SC) gap [17–22], the dynamics of electronic nematic fluctuations [11, 19, 23, 24], as well as the strength of electron-phonon interactions [25–28].

Recent discovery of a new class of stoichiometric and strictly tetragonal FeSCs $\text{CaAFe}_4\text{As}_4$ ($A = \text{K, Rb, Cs}$) with rather high T_c (31–36 K) provides an ideal platform for spectroscopic investigation of superconductors in clean limit, to decide on the role of nematicity for high T_c superconductivity in FeSCs [29–33]. Electron doping *via* substitution of Co or Ni for Fe, and/or application of pressure, suppresses T_c and induces an exotic spin-vortex crystal order, while the system remains tetragonal even for the magnetically ordered phase [34–36].

In this Letter, we report polarization-resolved Raman spectroscopic study of $\text{CaKFe}_4\text{As}_4$ single-crystals. In

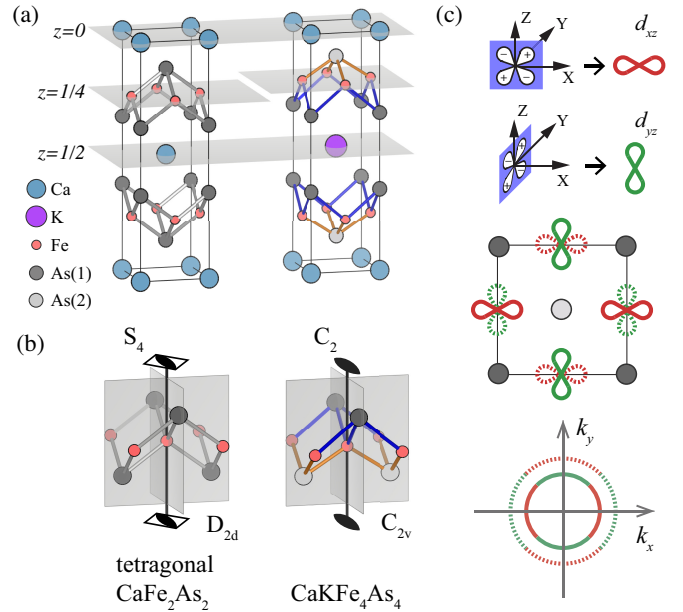


FIG. 1. (a) The comparison between CaFe_2As_2 and $\text{CaKFe}_4\text{As}_4$ lattice structures. For $\text{CaKFe}_4\text{As}_4$, the Fe sites are shifted away from the high symmetry $z=1/4$ and $3/4$ planes, causing two distinct As-Fe bond distances (shown in blue and orange). (b) The reduction of the Fe site-symmetry from D_{2d} for CaFe_2As_2 to C_{2v} for $\text{CaKFe}_4\text{As}_4$. (c) For $\text{CaKFe}_4\text{As}_4$, a sketch of the partially occupied d_{xz}/d_{yz} orbital order (the upper panel for real space), and derived two FS pockets in the vicinity of the Γ point (the lower panel for momentum space). Solid and dotted lines denote differences in the orbital occupation which induce a static quadrupole moment on the Fe sites with a checkerboard order.

contrast to the data from many FeSCs for which strong Pomeranchuk-like electronic nematic fluctuations give rise to intense electronic Raman continuum in the XY-quadrupole symmetry channel, the electronic Raman signal for $\text{CaKFe}_4\text{As}_4$ is weak and isotropic. Below T_c , we observe complete suppression of the low-frequency spectral intensity and development of three SC pair-breaking coherence peaks in the XY symmetry electronic Raman

response, which implies that all FS pockets are fully gapped. The pair-breaking peak energies $2\Delta = 13.8$, 16.9 and 21 meV are about 20% lower than twice the gap energies measured by single-particle spectroscopies. We attribute such renormalization to finite-state interactions in sub-dominant d -wave SC pairing channel. We also observe superconductivity induced phonon self-energy effect and estimate the electron-phonon (e-p) coupling to be weak, with coupling constant $\lambda^\Gamma = 0.0015$.

Crystallographic structure – The $\text{CaKFe}_4\text{As}_4$ single crystals ($T_c = 35$ K) used in this study were synthesized by flux method [29, 31]. The structure may be considered as a modification to the extensively studied tetragonal 122 FeSCs with the body-centered structure $I4/mmm$. For $\text{CaKFe}_4\text{As}_4$, every other plane of Ca atom is replaced by K, reducing the crystallographic space group to primitive $P4/mmm$ (point group D_{4h}) and therefore doubling the number of atoms in the primitive cell. In Figs. 1(a-b) we compare the tetragonal CaFe_2As_2 and $\text{CaKFe}_4\text{As}_4$ lattices.

For the body-centered CaFe_2As_2 , the Fe layers are at the high symmetry $z=1/4$ and $3/4$ planes, and each Fe has D_{2d} site symmetry with S_4 axis along z -direction, which imposes the degeneracy of Fe $3d_{xz}$ and $3d_{yz}$ orbitals. Such orbital degeneracy is a common feature for most of the FeSCs [37, 38]. It has been demonstrated that effect of partially filled d_{xz}/d_{yz} orbital degeneracy is significant: it causes dynamical charge oscillations between quasi-degenerate orbitals in sub-THz frequency range. This gives rise to fluctuating charge ferro-quadrupole moment with an amplitude proportional to the local oscillating charge imbalance $n_{xz} - n_{yz}$ [19]. The soft ferro-quadrupole fluctuations often show critical behavior leading to a d -wave Pomeranchuk instability [19, 39]. These fluctuations most dramatically manifest themselves in the low-frequency part of XY -symmetry Raman response as an overdamped quasi-elastic feature in the normal state [11, 19, 23] which undergoes a metamorphosis into a coherent in-gap collective mode below T_c [19–21, 40, 41].

In contrast, for $\text{CaKFe}_4\text{As}_4$ structure, the ordered alternating Ca and K layers above and below Fe-As layers cause the Fe positions shift away from the high symmetry planes [42, 43]. The shift gives rise to nonequivalent Fe-As bond distances for the As atoms above and below the Fe layer, thus, reducing the Fe site symmetry to C_{2v} (Fig. 1(a-b)). The removal of the S_4 symmetry on the Fe sites takes away the degeneracy of the partially occupied Fe d_{xz}/d_{yz} orbitals [42], giving rise to a static charge imbalance between these two orbitals, and, hence, creates a static $d_{x^2-y^2}$ -symmetry quadrupole moment on each Fe site. Because the orbital character of the lower energy state flips between two neighboring Fe sites, the structure forms a static checkerboard anti-quadrupole order (Fig. 1(c)). The stiffness of the static anti-quadrupole order parameter precludes Pomeranchuk-like fluctuations for the $\text{CaKFe}_4\text{As}_4$ compound.

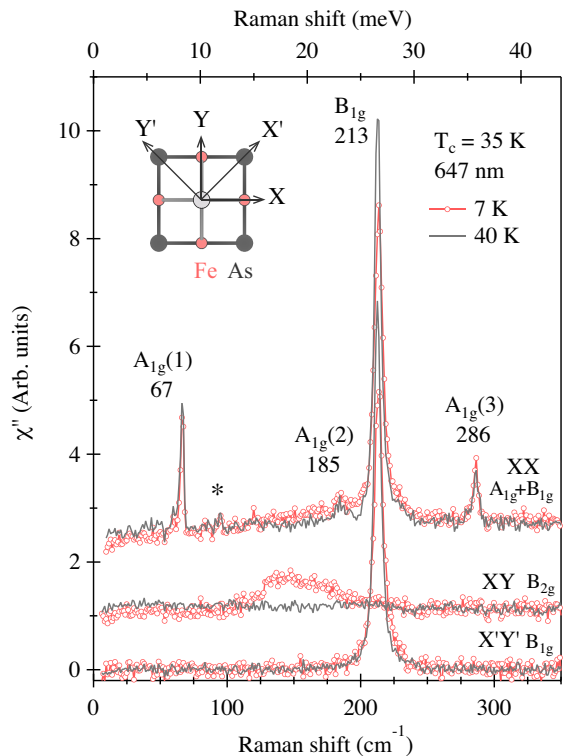


FIG. 2. Raman spectra for single crystal $\text{CaKFe}_4\text{As}_4$ at 40 and 7 K. The XY and XX polarized spectra are offset by 1 and 2 units, respectively. Inset: top view of the Fe-As layer and axes notation.

Experimental – Polarization-resolved Raman scattering measurements were performed in quasi-back scattering geometry from the natural cleaved (001) surface. We use $\mu\nu = XX$, XY and $X'Y'$ scattering geometries where $\mu\nu$ is short for $\bar{Z}(\mu\nu)Z$ in Porto's notation. These geometries allow coupling to excitations with the $A_{1g}+B_{1g}$ symmetry by XX polarization, B_{2g} symmetry by XY polarization, and B_{1g} symmetry by $X'Y'$ polarization.

The crystals were loaded into a continuous helium flow optical cryostat immediately after being cleaved in a nitrogen gas filled glove bag connected to the cryostat. We used the 647 nm line of a Kr^+ laser, where the laser beam was focused to a $50 \times 50 \mu\text{m}$ spot. The laser power was kept below 10 mW in the normal state and 2.3 mW for the SC state to reduce laser heating. The temperatures were corrected for the laser heating.

The Raman signal was collected and analyzed by a triple-grating spectrometer with 1.5 cm^{-1} spectral resolution. All spectra were corrected for spectral response and background determined from the $X'Y'$ symmetry electronic continuum to obtain the Raman scattering intensity $I_{\mu\nu}(\omega, T)$ [44]. The Raman response function $\chi''_{\mu\nu}(\omega, T)$ is related to $I_{\mu\nu}(\omega, T)$ by the Bose distribution factor $n(\omega, T)$: $I_{\mu\nu}(\omega, T) = [1+n(\omega, T)] \chi''_{\mu\nu}(\omega, T)$.

Raman continuum – In Fig. 2 we show Raman spectra at temperatures above and below T_c for XX , XY

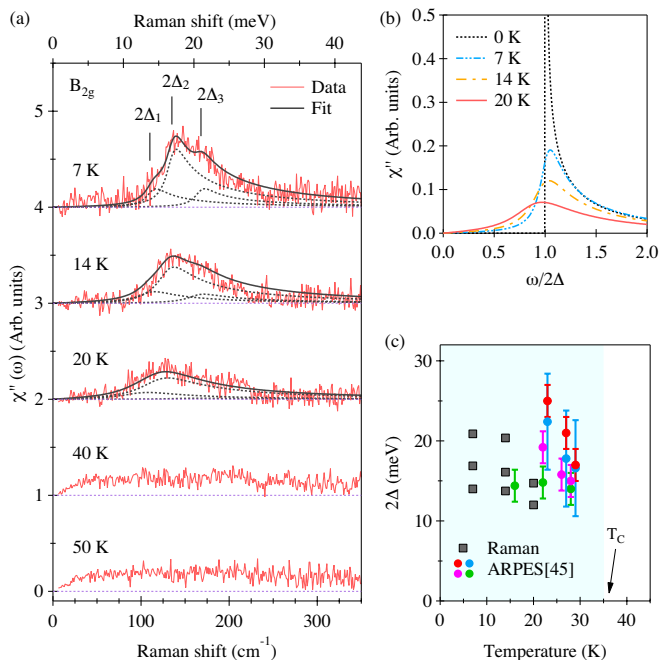


FIG. 3. (a) Temperature evolution of the B_{2g} symmetry Raman response. The black solid lines are fits to the data. Below T_c , the data are fit with three BCS gap response at finite temperature. (b) Temperature evolution of Raman response for a BCS gap. (c) The SC gap magnitude $2\Delta(T)$ measured by Raman spectroscopy and ARPES [45].

and $X'Y'$ polarizations. Above T_c , besides four sharp phonon modes, we observe a weak and featureless electronic continuum for all polarizations. Below T_c , for the XY scattering geometry, a broad feature appears at around 150 cm^{-1} , which is an indication of the SC gaps formation. For the XX and $X'Y'$ scattering geometries, the electronic continuum shows little change across T_c . In the following we focus on the electronic Raman response in the B_{2g} (XY) symmetry channel.

The common signature for most of the FeSCs is strong XY -symmetry Raman response. The enhancement of the Raman susceptibility has been attributed to the d_{XY} -symmetry Pomeranchuk-like fluctuations with Drude-like low-frequency response in the normal state and sharp in-gap collective mode in the superconducting state, both arising from strong oscillating charge ferro-quadrupole moments on the Fe sites due to the d_{xz}/d_{yz} orbital degeneracy [19, 46–48]. For $\text{CaKFe}_4\text{As}_4$ structure this orbital degeneracy is lifted, and because of that, the XY -symmetry Raman susceptibility is quite weak and featureless.

SC pair-breaking peaks – Below T_c , we observe a suppression of the low-frequency spectral weight and development of a feature between 10 to 30 meV. Upon cooling, the intensity and central frequency of this feature increase. At the lowest measured temperature (7 K), the spectral intensity below 12 meV is completely suppressed,

indicating that the SC gap is nodeless. We detect no SC coherence peak for a gap near 5 meV, as reported in Refs. [49, 50]. We note that the spectra does not display an in-gap collective mode which is a common feature for many FeSCs that show Pomeranchuk-like nematic fluctuations above T_c [19–21, 40].

We fit the data with three-gap model, $\chi'' = \sum_{i=1}^3 \alpha_i \chi_i''$. Here α_i denotes the spectral weight, and $\chi_i''(\omega, \Delta_i, T) = 4\Delta_i^2/\omega\sqrt{\omega^2 - 4\Delta_i^2} * L(\omega, T)$ denotes BCS coherence peaks with SC gap energies $2\Delta_i$ [17] convoluted with temperature dependent Lorentzian [51]. The effects of temperature broadening are depicted in Fig. 3(b).

In Fig. 3(c) we summarize the temperature dependence of the three SC gap amplitudes $2\Delta_i(T)$. At 7 K, the gaps energies 110 cm^{-1} (13.8 meV), 135 cm^{-1} (16.9 meV), and 168 cm^{-1} (21 meV) correspond to the $2\Delta/k_B T_c = 6.9, 5.5,$ and $4.5,$ ratios respectively. It appears that the pair-breaking peak energies measured by Raman are consistently near 20% lower than the gap energies determined for similar temperatures by ARPES [45]. We attribute this renormalization of the peak energies to the finite-state interaction effects in the sub-dominant d_{xy} -wave pairing channel [17, 40, 41].

Phonon self-energy effects – $\text{CaKFe}_4\text{As}_4$ crystal (point group D_{4h}) contains 10 atoms in a primitive cell. For phonons at the Γ point, group-theoretical symmetry decomposition yields $A_u + E_u$ acoustic modes, $4A_{2u} + 5E_u$ infrared active modes, $3A_{1g} + B_{1g} + 4E_g$ Raman active modes, and a B_{2u} silent mode. For the scattering experiments from (001) surface, we observe all three A_{1g} and a B_{1g} phonons (Fig. 2). The phonon energies and atomic displacements are summarized in Table I.

Above T_c all modes exhibit a conventional temperature dependence: hardening and narrowing upon cooling due to anharmonic decay [52–54]. However, we note that the behavior for the B_{1g} phonon mode in the SC state is anomalous: the mode’s energy and line width increase upon cooling, as shown in Fig. 4(a).

Similar phonon anomalies upon entering into SC state were reported for MgB_2 [28] and for cuprate superconductors [25, 26, 55–58]. The behavior was explained by Zeyher-Zwiczak’s model [27] which implies that in the presents of electron-phonon coupling, phonon self-energy is upward renormalized when the SC gap opens and the electronic density-of-states is pushed to the proximity of the phononic mode above the gaps energies.

TABLE I. Summary of Raman active phonons mode energies and atomic displacements for $\text{CaKFe}_4\text{As}_4$.

Symmetry	Energy at 40 K	Atomic displacements
$A_{1g}(1)$	67 cm^{-1}	$\text{Fe}(z) + \text{As}(1)(z) + \text{As}(2)(z)$
$A_{1g}(2)$	185 cm^{-1}	$\text{Fe}(z) + \text{As}(1)(z) + \text{As}(2)(z)$
$A_{1g}(3)$	286 cm^{-1}	$\text{Fe}(z) + \text{As}(1)(z) + \text{As}(2)(z)$
$B_{1g}(1)$	213 cm^{-1}	$\text{Fe}(z)$

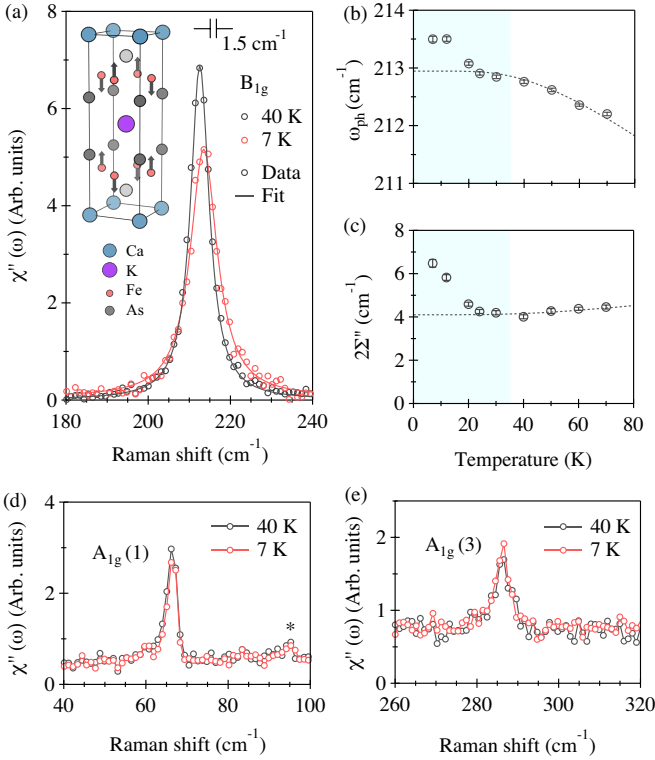


FIG. 4. Temperature evolution of phonon spectra. (a) The B_{1g} phonon spectra and the fitting curve for above (40 K) and below (7 K) T_c . Inset of (a): Atomic displacements of the B_{1g} phonon. (b)-(c) Temperature dependence of B_{1g} phonon energy ω_{ph} and line width $2\Sigma''$. Σ'' has been corrected for the spectrometer resolution as shown in (a). Dashed lines describe the anharmonic decay into two phonons obtained from the fit for the normal state. (d)-(e) The A_{1g}(1) and A_{1g}(3) phonon modes at 40 and 7 K.

It is interesting to note that in contrast to the 67 cm⁻¹ A_{1g} phonon (Fig.2) that exhibits an asymmetric Fano line shape, the B_{1g} phonon shows nearly perfect Lorentzian shape. We attribute this to weak Raman coupling to the B_{1g} symmetry electronic continuum: the e-p interaction only renormalizes the phonon self-energy without showing a Fano interference in the spectra.

To quantify the superconductivity induced self-energy effects and the e-p interaction strength, we fit the data with $\chi''_{ph}(\omega) \propto 4\omega_0\Sigma''[(\omega^2 - \omega_0^2 - 2\omega_0\Sigma')^2 + 4(\omega_0\Sigma'')^2]^{-1}$, where ω_0 is the bare phonon frequency, and $\Sigma = \Sigma' + i\Sigma''$ is complex phonon self-energy [27]. Thus, if Σ is small, the mode appears at $\omega_{ph} = \sqrt{\omega_0^2 + 2\omega_0\Sigma'}$ frequency. The fitting results are displayed in Figs. 4 (b-c) [54].

We calculate the coupling constant $\lambda_{B_{1g}}^\Gamma$ around Γ point [59]: $\lambda = -\kappa \sin u/u$, where $\kappa = [(\Sigma'(7K) - \Sigma'(40K)) - i(\Sigma''(7K) - \Sigma''(40K))]/\omega_{ph}(40K)$ and $u \equiv \pi + 2i \cosh^{-1}[\omega_{ph}(40K)/2\Delta]$. Using the energy of the strongest pair breaking peak $2\Delta = 135$ cm⁻¹, we acquire weak e-p coupling constant $\lambda_{B_{1g}}^\Gamma \approx 0.0015$. The A_{1g} phonons do not show measurable renormalization

(Figs. 4(d-e)). Therefore, the B_{1g} mode is the only phonon that exhibits the SC induced self-energy effects and the total e-p coupling constant λ can be approximated by $\lambda_{B_{1g}}^\Gamma$.

In comparison, for a conventional phonon-mediated superconductor MgB₂ with similar $T_c = 39$ K, a much larger coupling constant $\lambda = 0.2$ was derived from SC induced phonon renormalization [28]. Thus, for CaKFe₄As₄, the value λ is far from being sufficient to result in superconductivity with T_c at 35 K.

Conclusion – In summary, we report polarization-resolved Raman spectroscopic study of the single-crystal CaKFe₄As₄ superconductor with T_c at 35 K.

(1) We detect no signatures of Pomeranchuk-like electronic nematic fluctuations, which implies that the electronic nematicity may not be essential for high- T_c superconductivity in FeSCs.

(2) Below T_c , we observe complete suppression of low-frequency spectral weight and development of three SC pair-breaking peaks in the B_{2g} symmetry channel, which implies that all the SC gaps are nodeless. We do not detect in-gap collective modes which are commonly observed for FeSCs with strong electronic nematic fluctuations.

(3) The pair-breaking peaks energies are about 20% lower than twice SC gap energies measured by one-particle spectroscopy, likely due to finite-state interaction effects in the sub-dominant d_{xy} -symmetry pairing channel.

(4) We study the SC induced self-energy effects for Raman-active phonons and provide an estimate of the electron-phonon coupling constant $\lambda^\Gamma = 0.0015$, which is very small for a superconductor with T_c at 35 K.

By showing that the electronic nematic fluctuations and electron-phonon coupling are neglectfully small, we exclude them as a viable explanation for high- T_c superconductivity in CaKFe₄As₄. Naturally, one would consider the remaining spin-fluctuations to provide pairing interaction. In this case, the expected pairing symmetry is s_{\pm} , which is consistent with the observation of the spin-resonance mode at nesting vector (π, π) by inelastic neutron scattering [60].

Work at Rutgers was supported by the U.S. Department of Energy, Office of Basic Energy Sciences, Division of Materials Sciences and Engineering under Contract No. DE-SC0005463. Work at Ames Laboratory was supported by the U.S. Department of Energy, Office of Basic Energy Sciences, Division of Materials Sciences and Engineering under Contract No. DE-AC02-07CH11358. W.R.M was supported by the Gordon and Betty Moore Foundation's EPiQS Initiative through Grant No. GBMF4411.

- * wz131@physics.rutgers.edu
† girsh@physics.rutgers.edu
- [1] J. Paglione and R. L. Greene, *Nat Phys* **6**, 645 (2010).
 - [2] F. Wang and D.-H. Lee, *Science* **332**, 200 (2011).
 - [3] A. Chubukov, *Annu. Rev. Condens. Matter Phys.* **3**, 57 (2012).
 - [4] R. M. Fernandes, A. V. Chubukov, and J. Schmalian, *Nat. Phys.* **10**, 97 (2014).
 - [5] P. J. Hirschfeld, *Comptes Rendus Physique* **17**, 197 (2016).
 - [6] Q. Si, R. Yu, and E. Abrahams, *Nature Reviews Materials* **1**, 16017 (2016).
 - [7] T. Shibauchi, A. Carrington, and Y. Matsuda, *Annu. Rev. Condens. Matter Phys.* **5**, 113 (2014).
 - [8] I. I. Mazin, D. J. Singh, M. D. Johannes, and M. H. Du, *Phys. Rev. Lett.* **101**, 057003 (2008).
 - [9] P. J. Hirschfeld, M. M. Korshunov, and I. I. Mazin, *Rep. Prog. Phys.* **74**, 124508 (2011).
 - [10] J.-H. Chu, H.-H. Kuo, J. G. Analytis, and I. R. Fisher, *Science* **337**, 710 (2012).
 - [11] Y. Gallais, R. M. Fernandes, I. Paul, L. Chauvière, Y.-X. Yang, M.-A. Méasson, M. Cazayous, A. Sacuto, D. Colson, and A. Forget, *Phys. Rev. Lett.* **111**, 267001 (2013).
 - [12] H.-H. Kuo, J.-H. Chu, J. C. Palmstrom, S. A. Kivelson, and I. R. Fisher, *Science* **352**, 958 (2016).
 - [13] S. Lederer, Y. Schattner, E. Berg, and S. A. Kivelson, *Phys. Rev. Lett.* **114**, 097001 (2015).
 - [14] H. Kontani and S. Onari, *Phys. Rev. Lett.* **104**, 157001 (2010).
 - [15] W.-G. Yin, C.-C. Lee, and W. Ku, *Phys. Rev. Lett.* **105**, 107004 (2010).
 - [16] T. Saito, S. Onari, and H. Kontani, *Phys. Rev. B* **82**, 144510 (2010).
 - [17] M. V. Klein and S. B. Dierker, *Phys. Rev. B* **29**, 4976 (1984).
 - [18] T. P. Devereaux and R. Hackl, *Rev. Mod. Phys.* **79**, 175 (2007), and refs therein.
 - [19] V. K. Thorsmølle, M. Khodas, Z. P. Yin, C. Zhang, S. V. Carr, P. Dai, and G. Blumberg, *Phys. Rev. B* **93**, 054515 (2016).
 - [20] Y. Gallais, I. Paul, L. Chauvière, and J. Schmalian, *Phys. Rev. Lett.* **116**, 017001 (2016).
 - [21] S.-F. Wu, P. Richard, H. Ding, H.-H. Wen, G. Tan, M. Wang, C. Zhang, P. Dai, and G. Blumberg, *Phys. Rev. B* **95**, 085125 (2017).
 - [22] T. Böhm, F. Kretzschmar, A. Baum, M. Rehm, D. Jost, R. Hosseinian Ahangharnejhad, R. Thomale, C. Platt, T. A. Maier, W. Hanke, B. Moritz, T. P. Devereaux, D. J. Scalapino, S. Maiti, P. J. Hirschfeld, P. Adelman, T. Wolf, H.-H. Wen, and R. Hackl, ArXiv e-prints (2017), [arXiv:1703.07749](https://arxiv.org/abs/1703.07749).
 - [23] F. Kretzschmar, T. Böhm, U. Karahasanovic, B. Muschler, A. Baum, D. Jost, J. Schmalian, S. Caprara, M. Grilli, C. Di Castro, J. G. Analytis, J. H. Chu, I. R. Fisher, and R. Hackl, *Nat. Phys.* **12**, 560 (2016).
 - [24] S.-F. Wu, W.-L. Zhang, L. Li, H. B. Cao, H.-H. Kung, A. S. Sefat, H. Ding, P. Richard, and G. Blumberg, ArXiv e-prints (2017), [arXiv:1712.06066](https://arxiv.org/abs/1712.06066).
 - [25] S. L. Cooper, M. V. Klein, B. G. Pazol, J. P. Rice, and D. M. Ginsberg, *Phys. Rev. B* **37**, 5920 (1988).
 - [26] C. Thomsen, M. Cardona, B. Gegenheimer, R. Liu, and A. Simon, *Phys. Rev. B* **37**, 9860 (1988).
 - [27] R. Zeyher and G. Zwirgagl, *Z. Phys. B* **78**, 175 (1990).
 - [28] A. Mialitsin, B. S. Dennis, N. D. Zhigadlo, J. Karpinski, and G. Blumberg, *Phys. Rev. B* **75**, 020509 (2007).
 - [29] W. R. Meier, T. Kong, U. S. Kaluarachchi, V. Taufour, N. H. Jo, G. Drachuck, A. E. Böhmer, S. M. Saunders, A. Sapkota, A. Kreyssig, M. A. Tanatar, R. Prozorov, A. I. Goldman, F. F. Balakirev, A. Gurevich, S. L. Bud'ko, and P. C. Canfield, *Phys. Rev. B* **94**, 064501 (2016).
 - [30] A. Iyo, K. Kawashima, T. Kinjo, T. Nishio, S. Ishida, H. Fujihisa, Y. Gotoh, K. Kihou, H. Eisaki, and Y. Yoshida, *J. Amer. Chem. Soc.* **138**, 3410 (2016).
 - [31] W. R. Meier, T. Kong, S. L. Bud'ko, and P. C. Canfield, *Phys. Rev. Materials* **1**, 013401 (2017).
 - [32] R. Yang, Y. Dai, B. Xu, W. Zhang, Z. Qiu, Q. Sui, C. C. Homes, and X. Qiu, *Phys. Rev. B* **95**, 064506 (2017).
 - [33] K. Kawashima, S. Ishida, H. Fujihisa, Y. Gotoh, K. Kihou, Y. Yoshida, H. Eisaki, H. Ogino, and A. Iyo, *J. Phys. Chem. Lett.* **9**, 868 (2018).
 - [34] W. R. Meier, Q.-P. Ding, A. Kreyssig, S. L. Bud'ko, A. Sapkota, K. Kothapalli, V. Borisov, R. Valentí, C. D. Batista, P. P. Orth, R. M. Fernandes, A. I. Goldman, Y. Furukawa, A. E. Böhmer, and P. C. Canfield, *npj Quantum Materials* **3**, 5 (2018).
 - [35] U. S. Kaluarachchi, V. Taufour, A. Sapkota, V. Borisov, T. Kong, W. R. Meier, K. Kothapalli, B. G. Ueland, A. Kreyssig, R. Valentí, R. J. McQueeney, A. I. Goldman, S. L. Bud'ko, and P. C. Canfield, *Phys. Rev. B* **96**, 140501 (2017).
 - [36] L. Xiang, W. R. Meier, M. Xu, U. S. Kaluarachchi, S. L. Bud'ko, and P. C. Canfield, ArXiv e-prints (2018), [arXiv:1803.10733](https://arxiv.org/abs/1803.10733).
 - [37] V. Cvetkovic and O. Vafek, *Phys. Rev. B* **88**, 134510 (2013).
 - [38] J. Hu and N. Hao, *Phys. Rev. X* **2**, 021009 (2012).
 - [39] Y. A. Pomeranchuk, *Sov. Phys. JETP* **8**, 361 (1958).
 - [40] M. Khodas, A. V. Chubukov, and G. Blumberg, *Phys. Rev. B* **89**, 245134 (2014).
 - [41] S. Maiti, A. V. Chubukov, and P. J. Hirschfeld, *Phys. Rev. B* **96**, 014503 (2017).
 - [42] F. Lochner, F. Ahn, T. Hickel, and I. Eremin, *Phys. Rev. B* **96**, 094521 (2017).
 - [43] J. Cui, Q.-P. Ding, W. R. Meier, A. E. Böhmer, T. Kong, V. Borisov, Y. Lee, S. L. Bud'ko, R. Valentí, P. C. Canfield, and Y. Furukawa, *Phys. Rev. B* **96**, 104512 (2017).
 - [44] The background is determined from the $X'Y'$ symmetry scattering intensity after subtracting the B_{1g} phonon, see supplement I in [61].
 - [45] D. Mou, T. Kong, W. R. Meier, F. Lochner, L.-L. Wang, Q. Lin, Y. Wu, S. L. Bud'ko, I. Eremin, D. D. Johnson, P. C. Canfield, and A. Kaminski, *Phys. Rev. Lett.* **117**, 277001 (2016).
 - [46] H. Yamase, *Phys. Rev. Lett.* **93**, 266404 (2004).
 - [47] H. Yamase and R. Zeyher, *Phys. Rev. B* **83**, 115116 (2011).
 - [48] H. Yamase and R. Zeyher, *Phys. Rev. B* **88**, 125120 (2013).
 - [49] P. K. Biswas, A. Iyo, Y. Yoshida, H. Eisaki, K. Kawashima, and A. D. Hillier, *Phys. Rev. B* **95**, 140505 (2017).
 - [50] K. Cho, A. Fente, S. Teknowijoyo, M. A. Tanatar, K. R. Joshi, N. M. Nusran, T. Kong, W. R. Meier, U. Kaluarachchi, I. Guillamón, H. Suderow, S. L. Bud'ko, P. C.

- Canfield, and R. Prozorov, *Phys. Rev. B* **95**, 100502 (2017).
- [51] G. Blumberg, A. Mialitsin, B. Dennis, N. Zhigadlo, and J. Karpinski, *Physica C: Superconductivity* **456**, 75 (2007).
- [52] P. G. Klemens, *Phys. Rev.* **148**, 845 (1966).
- [53] J. Menéndez and M. Cardona, *Phys. Rev. B* **29**, 2051 (1984).
- [54] $\omega_{ph}(T) = \omega_{ph}(0) - \omega_1(1 + 2/\exp(\omega_{ph}(0)/k_B T) - 1)$, $\Sigma''(T) = \Sigma''(0) + \Gamma_1(1 + 2/(\exp(\omega_{ph}(0)/k_B T) - 1))$ are used to fit $\omega_{ph}(T)$ and $\Sigma''(T)$ for the normal state [52]. The dashed curves in Figs. 4b-c are plotted with the fitting result $\omega_{ph}(0) = 216.0 \pm 0.1 \text{ cm}^{-1}$, $\omega_1 = 3.1 \pm 0.1 \text{ cm}^{-1}$, $\Sigma''(0) = 2.2 \pm 0.3 \text{ cm}^{-1}$, and $\Gamma_1 = 0.6 \pm 0.3 \text{ cm}^{-1}$.
- [55] B. Friedl, C. Thomsen, and M. Cardona, *Phys. Rev. Lett.* **65**, 915 (1990).
- [56] K. F. McCarty, H. B. Radousky, J. Z. Liu, and R. N. Shelton, *Phys. Rev. B* **43**, 13751 (1991).
- [57] G. Blumberg, M. V. Klein, L. Börjesson, R. Liang, and W. N. Hardy, *J. Supercond.* **7**, 445 (1994).
- [58] C. Thomsen and M. Cardona, "Raman scattering in high-*T*c superconductors," in *Physical Properties of High Temperature Superconductors I*, Chap. 8, pp. 409–507.
- [59] C. O. Rodriguez, A. I. Liechtenstein, I. I. Mazin, O. Jepsen, O. K. Andersen, and M. Methfessel, *Phys. Rev. B* **42**, 2692 (1990).
- [60] K. Iida, M. Ishikado, Y. Nagai, H. Yoshida, A. D. Christianson, N. Murai, K. Kawashima, Y. Yoshida, H. Eisaki, and A. Iyo, *J. Phys. Soc. Jpn.* **86**, 093703 (2017).
- [61] W.-L. Zhang, S.-F. Wu, S. Kasahara, T. Shibauchi, Y. Matsuda, and G. Blumberg, ArXiv e-prints (2017), [arXiv:1710.09892](https://arxiv.org/abs/1710.09892).